


Determination of Charge-Carrier Mobility in Disordered Thin-Film Solar Cells as a Function of Current Density

Helmut Mäckel^{1,*} and Roderick C. I. MacKenzie²

¹*Independent Researcher, Koboldstraße 26a, 81739 München, Germany*

²*Faculty of Engineering, University of Nottingham, Nottingham, Nottinghamshire NG7 2RD, United Kingdom*

 (Received 3 October 2016; revised manuscript received 3 October 2017; published 23 March 2018)

Charge-carrier mobility is a fundamental material parameter, which plays an important role in determining solar-cell efficiency. The higher the mobility, the less time a charge carrier will spend in a device and the less likely it is that it will be lost to recombination. Despite the importance of this physical property, it is notoriously difficult to measure accurately in disordered thin-film solar cells under operating conditions. We, therefore, investigate a method previously proposed in the literature for the determination of mobility as a function of current density. The method is based on a simple analytical model that relates the mobility to carrier density and transport resistance. By revising the theoretical background of the method, we clearly demonstrate what type of mobility can be extracted (constant mobility or effective mobility of electrons and holes). We generalize the method to any combination of measurements that is able to determine the mean electron and hole carrier density, and the transport resistance at a given current density. We explore the robustness of the method by simulating typical organic solar-cell structures with a variety of physical properties, including unbalanced mobilities, unbalanced carrier densities, and for high or low carrier trapping rates. The simulations reveal that near V_{OC} and J_{SC} , the method fails due to the limitation of determining the transport resistance. However, away from these regions (and, importantly, around the maximum power point), the method can accurately determine charge-carrier mobility. In the presence of strong carrier trapping, the method overestimates the effective mobility due to an underestimation of the carrier density.

DOI: [10.1103/PhysRevApplied.9.034020](https://doi.org/10.1103/PhysRevApplied.9.034020)

I. INTRODUCTION

Thin-film solar cells based on disordered materials such as organic carbon-based conducting molecules or amorphous inorganic semiconductors have great potential as a low-cost, low-carbon source of electricity. For such devices to be efficient, the photoabsorber must be able to efficiently transport charge to enable low resistive losses and reduced current loss via recombination. The figure of merit for charge transport is charge-carrier mobility. In traditional inorganic semiconductors, this mobility can be as high as $4 \times 10^3 \text{ cm}^2/(\text{Vs})$, while in disordered materials, it is typically in the range of 10^{-5} – $10^{-4} \text{ cm}^2/(\text{Vs})$. A low mobility will reduce the fill factor (FF), short-circuit currents, and open-circuit voltage [1,2]. Unfortunately, even for nominally identical disordered materials, there exists a large variation of reported charge-carrier mobility values, with the reported values depending strongly upon the measurement technique employed [3,4]. Part of the reason for this variation is that carrier mobility is a strong function of carrier density in these disordered material systems. This is

because at low carrier densities, proportionally more deep trap states will be occupied, and, thus, on average it will be energetically difficult for charge carriers to move. As the charge density is increased due to the Pauli exclusion principle, higher states will be filled where transport is energetically easier [5–11]. However, many measurement techniques inherently neglect this dependence. Furthermore, the measurement conditions (such as applied-bias voltage, light intensity, or device geometry) vary from method to method. This also means that charge-carrier density varies from method to method, making it difficult to compare mobility values between material systems. This creates the need for a reproducible measurement technique, which can consistently measure charge-carrier mobility as a function of charge-carrier density. Furthermore, it should be noted that for mobility to be a useful figure of merit for a light-harvesting device, values should be compared at the maximum power point under steady-state operating conditions; hence, there is a need to be able to reliably evaluate mobility as a function of current. Finally, before going further, it should be noted that measuring mobility in disordered semiconductors is a difficult problem to solve due to the charge-carrier mobility being a function of carrier density and the fact

*helmut.maeckel@gmail.com

that often in disordered materials, any change in device structure (even a change in bottom contact) can change the morphology or electrical properties of the subsequently deposited layers. Thus, it is difficult to use techniques from inorganic semiconductor physics, such as Hall probe measurements, which require special device structures to be fabricated. Consequently, experimentalists have had to come up with ingenious methods to tease mobility out of working devices.

The most common methods to determine mobility are steady-state space-charge-limited current (SCLC) [12], time of flight (TOF) [13], dark-injection transient current (DITC) [14], and charge extraction by linearly increasing voltage (CELIV) [15]. TOF, DITC, and CELIV assume a mobility independent of carrier density and suffer from several drawbacks: For TOF, the dielectric relaxation time must be larger than the transit time. Moreover, the experiment has to be performed at high negative-bias voltage, meaning the background charge density will be lower than is found in an operating device. Finally, photogenerated charges have to be produced close to one electrode. Therefore, the device must be optically thick (around $1\ \mu\text{m}$), and as material microstructure is often a function of thickness, this makes it difficult to measure functioning solar cells which are typically only $100\ \text{nm}$ thin [15]. For the DITC method, pulse parameters such as pulse on and off times have the potential to significantly affect the value of measured mobility due to charge trapping and detrapping effects [16,17]. Furthermore, the models commonly used to interpret the results do not take these trapping effects into account. For CELIV, simulations of organic solar cells have shown that the technique is only able to determine an apparent mobility, which can be up to 2 orders of magnitude different from the actual mobility of the faster carriers [18]. The reason is rooted in the basic assumptions made for the theory behind CELIV. Most important, it requires that the carrier distribution inside the photoactive layer is given by a uniform sheet of charge carriers, which is neatly swept out of the device by the applied voltage. However, due to disorder, most charges in disordered materials reside in trap states. Hence, the extraction of charge carriers is altered by trapping and detrapping of charge carriers. As a result, the shape of the CELIV curve is affected by the density and distribution of these trap states and the average carrier mobility changes during the CELIV measurement.

Unlike the above techniques, with SCLC, the carrier dependence of mobilities can be determined [5,6,8]. However, the great disadvantage of SCLC is that a hole-only or electron-only diode structure is required. Very often, in thin-film devices the electrical properties of the layer will depend on how the material is deposited (or even on which layer it is being deposited), and even nominally identical devices can have differing mobilities. Furthermore, many organic solar cells rely on a bulk heterojunction absorber with a closely intermixed network of donor and acceptor

components. In these devices, charge transport is by definition ambipolar [4]. Additionally, the built-in voltage and dielectric constant must be known to apply this technique, the former being especially difficult to measure in disordered devices [19]. Finally, another drawback of SCLC is the difficulty of distinguishing between injection-limited and space-charge-limited currents.

In 2010, Shuttle *et al.* [7] proposed a method to determine the mobility as a function of carrier density. It is based on the charge-extraction (CE) measurement [20] in which the solar cell is first held at short circuit under illumination. The light source is then switched off and the device simultaneously short circuited. Provided that recombination losses are negligible, the integral of the current leaving the device is a measure of the excess charge in the cell. By varying the bias-light intensity, one can explore a range of carrier densities, and with the aid of an analytical model, carrier-density-dependent mobility can be extracted. Even though the method is attractive because of its simplicity, it suffers from several drawbacks: the mobility is accessible only at short-circuit condition, the analytical model assumes that transport is driven only by one type of carrier, it requires knowledge of the built-in potential, and it does not account for diffusion.

Albrecht *et al.* [21] extended Shuttle's method so that any forward-bias condition could be used. Errors due to recombination between the steady-state illumination and the transient charge extraction were minimized by rapidly applying a high reverse bias after switching off the light. The method is based on the following relationship among mobility, carrier density, and transport resistance:

$$\mu_{\text{eff}} = \frac{d}{2q\bar{n}R_{\text{tr}}}. \quad (1)$$

Here, μ_{eff} is an effective mobility of electrons and holes, J the current density, d the device thickness, q the elemental charge, and \bar{n} the average carrier density extracted from the measurement. R_{tr} is the resistance caused by the transport of electron and holes through the device. In the technique by Albrecht *et al.*, charge-extraction measurements are performed at two different measurement conditions. Under the first condition, a forward bias is applied to the device under a given light intensity before performing charge extraction. Under the second, the device is held at open circuit before performing charge extraction. For this condition, the light intensity is varied until the extracted carrier density matches the one of the first condition. From the voltage differences of these two measurements, R_{tr} is estimated. Together with \bar{n} , this allows the determination of the mobility as a function of current density. Albeit, the method requires about twice as many measurement steps as the one by Shuttle *et al.*, but it is not hampered by the assumptions made therein. Hence, neither the built-in voltage has to be known nor has one to assume that transport is dominated by one type of carrier or only by drift.

However, the underlying analytical model proposed by Albrecht is afflicted by several assumptions, which limit the general applicability of the method. First, in Eq. (1) it is assumed that the electron and hole current densities are equal throughout the device. However, this assumption is generally not true. Second, the theoretical \bar{n} in their formula is equal to the geometrical mean of the electron and hole densities, while the measurement extracts the arithmetic mean. This leads to an underestimation of the effective mobility. Next, it neglects the voltage drop across the outer circuitry. Finally, Eq. (1) is only valid for the simplification $\bar{n}_{e(h)} = n_{e(h)} = \text{const}$. This assumes that the carrier density across the device is uniform, when in fact, in many cases it exponentially decays away from the contacts.

Equation (1) was also independently established by Schiefer *et al.* using another approach [22]. They assumed a constant and equal mobility for electrons and holes, which they determined via CELIV. R_{tr} was extracted from a combination of a light J - V curve and Suns- V_{OC} curve. With the help of Eq. (1), they were then able to determine the average carrier density. The approach by Schiefer *et al.* extracts the transport resistance correctly, but it assumes that the average electron and hole current densities are equal and contribute equally to the total current. Furthermore, their approach is limited to the case $\bar{\mu}_h = \bar{\mu}_e = \text{const}$ and $\bar{n}_h = \bar{n}_e = \bar{n}$; however, mobility is known to be a strong function of carrier density, and as we state above, the carrier density decreases exponentially as the distance from the contact is increased.

In this work, we present a simulation study that critically investigates the work of Albrecht *et al.* and Schiefer *et al.* Revising the derivation of Eq. (1), we demonstrate that the effective mobility is, in general, a function of the spatially dependent carrier densities. The method is generalized to any combination of measurements that is able to determine the arithmetic mean of the average carrier density of electron and holes, and the transport resistance at a given current density. Drift-diffusion simulations of typical organic solar-cell structures are used to critically assess the advantages and limitations of the method.

This paper is organized as follows: First, we investigate reliability of measuring charge density using the transient photovoltage (TPV) and transient photocurrent (TPC). Then, for a combination of J - V and transient measurements, we revisit and generalize the theory behind Eq. (1) for the extraction of the mobility. Thereafter, we examine the conditions under which Eq. (1) is valid and where it is not.

II. MEASURING CHARGE-CARRIER DENSITY

For the measurement of the charge-carrier density, two widely employed techniques are equally appropriate: charge extraction as presented by Albrecht *et al.* or a combination of TPV and TPC measurements [23]. Charge extraction has the advantage that only one measurement has

to be performed at each current density. However, a general drawback of charge extraction is the practical aspect of turning off a 1-sun light source and shorting a steady-state solar cell quickly enough as not to influence the measured current transient. Furthermore, the more quickly the cell and light source are switched, the more pronounced inductive ringing and rf effects become in the charge-extraction transients. By using a method called differential charging [23], where TPV and TPC are used together to determine charge density, one needs two measurements at each current density. However, the method is a small-signal method, so one avoids the parasitic effects associated with large-signal measurements. Furthermore, TPV will also provide carrier-lifetime information at the same time, which can be used to calculate diffusion lengths, another important figure of merit. For the above reasons, for this work we choose the combination of TPV and TPC.

The use of transient voltage and current techniques to measure the carrier lifetime of minority charge carriers in p - n junctions has a long history [24]. They are generally called open-circuit voltage decay (OCVD) and short-circuit current decay (SCCD). When applied to dye-sensitized solar cells (DSSCs), the techniques were more recently dubbed transient photovoltage and transient photocurrent, respectively. These terms now prevail throughout the DSSC, organic photovoltaic, and other novel thin-film solar-cell literature. TPV is mainly used to determine the carrier lifetime [25–27], while TPC is chiefly applied to study trapping and detrapping effects [28–30].

In this work, we make use of both the transient voltage and current techniques, where a steady-state bias light is used in conjunction with a small perturbation light source [23,30]. The steady-state bias light is a white-light source, while the small excitation light source may be a laser or a single-wavelength LED. Its wavelength range should be selected in a way so that the generation profile is as uniform as possible in the device. For this investigation, we opt for a laser of wavelength 370 nm with a short pulse width of 5 ns. In the following, we denote quantities related to the small perturbation pulse, for example, a small change in carrier density, with the term “excess” or “ Δ .” This is to distinguish these quantities from their steady-state counterparts.

Figure 1 illustrates a typical simulation of TPV and TPC experiments and the information extracted from them. The upper left panel depicts a TPV experiment, while the lower left panel depicts a TPC experiment. The illumination induces the generation of charge carriers in the device, which is plotted as a red line in Figs. 1(a) and 1(b). At the start of the experiment, the device is illuminated with a steady-state bias light until an equilibrium between generation, recombination, and in the case of TPC, extraction is reached. Thereafter, an additional small light pulse is applied to the device, which is discernible by the vertical red line in Figs. 1(a) and 1(b). When the device is held under open circuit, the bias light produces a bias voltage

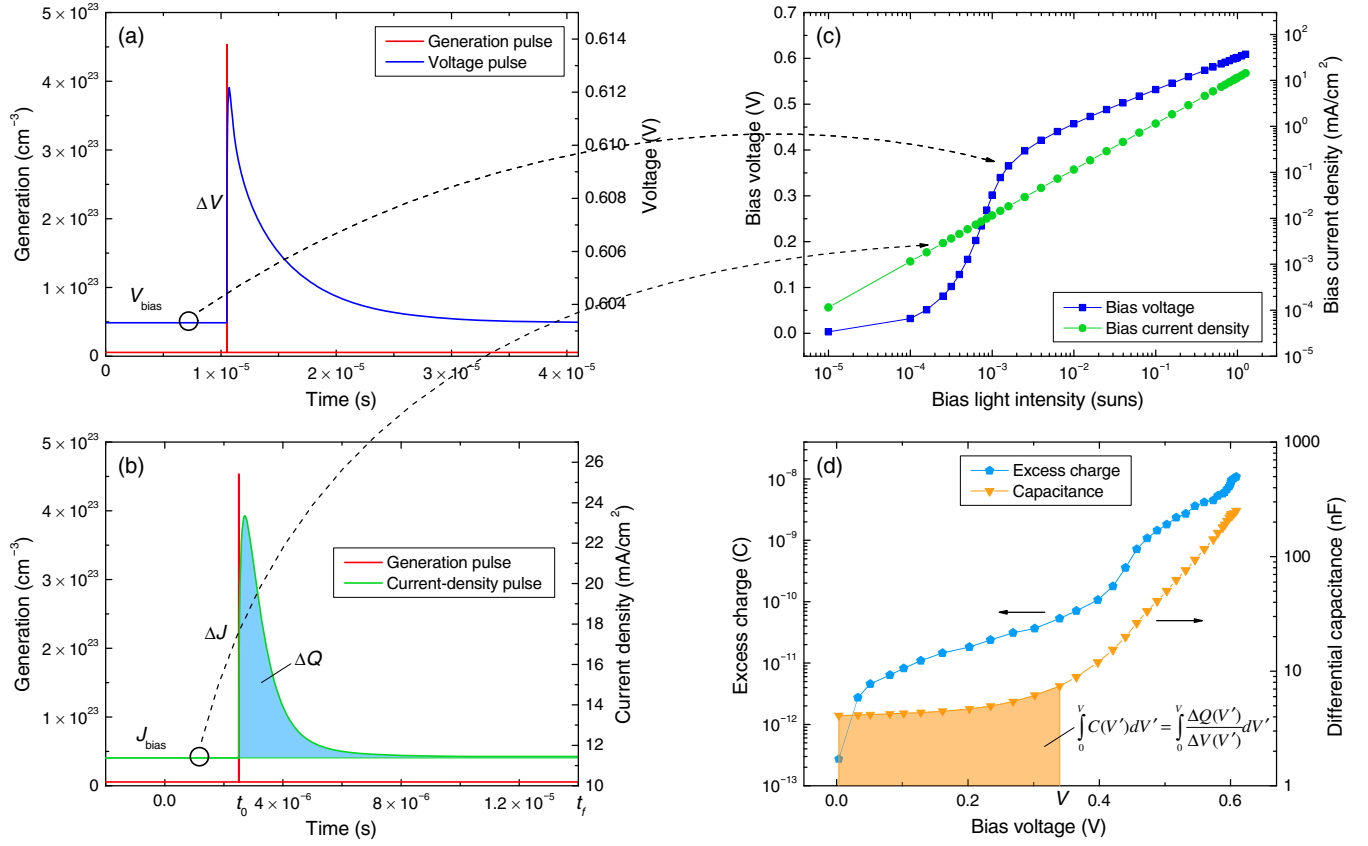


FIG. 1. Illustration of typical TPV and TPC simulations and the parameters extracted from them. (a) TPV simulation: The red line depicts the generation rate consisting of a steady-state generation and a small-signal pulse. The blue line is the photovoltage response, which is composed of the steady-state bias voltage V_{bias} , a small excitation voltage ΔV , and the monoexponential decay after the small-signal excitation has been switched off. (b) TPC simulation: The red line shows the same generation rate as in (a). The green line exhibits the TPC response, which is also made up of the steady-state bias-current density J_{bias} , a small-signal current density ΔJ , and an exponential decay after switching off the small-signal excitation. The light blue area under the current transient is the excess charge ΔQ extracted during the small-signal perturbation. (c) V_{bias} and J_{bias} as a function of bias-light intensity I_{light} . They are extracted from bias-light-dependent TPV and TPC simulations, respectively. (d) Excess charge ΔQ and differential capacitance $C = \Delta Q/\Delta V$ as a function of bias voltage. ΔQ is determined from a bias-light-dependent TPC simulation; see (b). ΔV is computed from an adjoined TPV simulation; see (a). The light orange area under the capacitance-voltage curve is proportional to the total photoinduced carrier density at the upper limit of the integration V .

V_{bias} ; under short-circuit conditions, a bias current J_{bias} is established. The small perturbation light generates excess charge carriers, which is manifested by an excess voltage ΔV or excess current density ΔJ . After switching off the small light source, the voltage and current density decay exponentially until they reach their bias values. In the case of TPV, the voltage decay is caused by recombination and trapping. In the case of TPC, the current decays since the majority of the excess charge carriers are extracted out of the device. The intensity of the small excitation light is attenuated so that the perturbation is small compared to the bias-light intensity. For TPV, this is to ensure that the voltage transient takes the form of a single exponential [23]. Its decay time can be interpreted as the carrier lifetime of the small excitation carriers [23,31]. The data are usually read out by an oscilloscope using the 1-M Ω input terminal for TPV and the 50- Ω input terminal for TPC.

By varying the intensity of the steady-state light source I_{light} , the bias-light-dependent parameters can be determined. When I_{light} is independently measured by a calibrated photodetector, V_{bias} or J_{bias} can be plotted against the intensity. This is illustrated in Fig. 1(c) for a simulation of bias-light-dependent TPV and TPC measurements. The V_{bias} -intensity curve shows the typical shape of a diode's J - V curve in the dark. It is also known as Suns- V_{OC} curve [32], and we later use it to construct a J_{SC} - V_{OC} curve, which is needed for the determination of the mobility. The J_{bias} -intensity curve, in turn, reveals a linear dependence between light intensity and bias-current density.

By a combination of TPV and TPC measurements, the excess carrier density can be deduced employing a method known as *differential charging* [23]. During a current transient of a TPC measurement, an excess charge ΔQ or average excess carrier density $\Delta \bar{n}_{\text{TPC}}$ is extracted from

the device. In a first approximation, it can be obtained by integrating the area under the short-circuit current transient [shown by the light blue area in Fig. 1(b)],

$$\Delta Q = Adq\Delta\bar{n}_{\text{TPC}} \approx A \int_{t_0}^{t_f} \Delta J dt, \quad (2)$$

where A is the device area, d the device thickness, q the elemental charge, and t_0 and t_f are the start and finish of the current transient, respectively [Fig. 1(b)]. In a TPV measurement performed under the same illumination conditions, the small-signal perturbation induces a photovoltage peak ΔV [Fig. 1(a)]. We can, therefore, define a capacitance for the device at any given measurement condition as $C = \Delta Q/\Delta V$; ΔQ and C are depicted in Fig. 1(d) as a function of bias voltage. It can be seen that both ΔQ and C exhibit a strong dependence upon V_{bias} . Now, *differential charging* assumes that, starting from dark conditions, the average excess carrier density can be calculated by summing CdV while increasing the light bias in small steps. dV signifies here the increase of V_{bias} between successive measurement steps. Integrating C with respect to the voltage gives the expression for the average carrier density $\bar{n}_{\text{TPV,TPC}}$ as a function of voltage:

$$\bar{n}_{\text{TPV,TPC}}(V) = \frac{1}{Aqd} \int_0^V C(V') dV'. \quad (3)$$

This integration is depicted in Fig. 1(d) by the light orange area. It is clear from this derivation that $\bar{n}_{\text{TPV,TPC}}$ is only composed of photoinduced charge carriers and does not include the dark carrier density. When the bias-light intensity is varied, the dependence of the carrier lifetime on excess carrier density can be determined [23]. From this dependence, other recombination parameters such as the recombination rate, coefficient, or order can be revealed. Here, we use bias-light-dependent TPV and TPC measurements as a means of determining the carrier density $\bar{n}_{\text{TPV,TPC}}$, and from there, the mobility, as we explain in the next section.

The determination of $\Delta\bar{n}_{\text{TPC}}$ is only valid under certain conditions. A theoretical derivation reveals the following relationship between the integrated area under the current transient and the charge-carrier dynamics [33]:

$$\frac{1}{Aqd} \int_{t_0}^{t_f} \Delta I_{\text{SC}} dt = \frac{1}{2} (\Delta\bar{n}_{e,\text{init}} + \Delta\bar{n}_{h,\text{init}}) - \frac{\Delta\sigma_{\text{EL}}}{2qd} - \int_{t_0}^{t_f} \left(\frac{\Delta J_{\text{surf}}}{qd} + \Delta R \right) dt. \quad (4)$$

Here, $\Delta\bar{n}_{e(h),\text{init}} = \Delta\bar{n}_{e(h)}|_{t_0} - \Delta\bar{n}_{e(h)}|_{t_f}$ denotes the average excess carrier density, which is initially generated due to the small-signal pulse. $\Delta\sigma_{\text{EL}}$ is defined as the change in charge on the contacts

$$\Delta\sigma_{\text{EL}} = (\sigma_d - \sigma_0)|_{t_0} - (\sigma_d - \sigma_0)|_{t_f}, \quad (5)$$

where σ_d and σ_0 are the charge densities (in cm^2) on the left and right metal electrodes, respectively. $\Delta J_{\text{surf}} = \Delta J_n(0) + \Delta J_p(d)$ is the total excess surface recombination current density due to net electron extraction at the hole-selective contact $\Delta J_n(0)$ and net hole extraction at the electron-selective contact $\Delta J_p(d)$. ΔR is the total excess recombination rate due to trapping and Shockley-Read-Hall recombination [33]. With device simulations, we analyze the contribution of each component of the right-hand side of Eq. (4) to the integral under the current transient. For the later discussion, we, therefore, express Eq. (4) in terms of excess carrier densities:

$$\Delta n_{\text{TPC}} = \Delta n_{\text{init}} - \Delta n_{\text{EL}} - \Delta n_{\text{surf}} - \Delta n_R, \quad (6)$$

where we combine the initially generated excess carrier density of electrons and holes in the term Δn_{init} . Δn_{EL} corresponds to the change in the carrier densities on the contacts. Δn_{surf} and Δn_R stand for the excess carrier densities lost due to surface and bulk recombination, respectively. Thus, Δn_{TPC} is equal to Δn_{init} if surface and bulk recombination, and the change in charge on the contacts can be ignored. We like to stress the fact that Δn_{TPC} is then equal to half the sum of the initial electron and hole carrier density. This result is derived for any kind of current transient [33] and is, thus, also applicable to the charge-extraction method.

III. DETERMINATION OF THE MOBILITY

The concept of mobility in disordered materials is less straightforward than in crystalline semiconductors. Crystalline semiconductors possess a highly ordered regular arrangement of atoms, and Bloch's theory tells us that this will produce well-defined transport bands with a forbidden region separating them (the band gap). Disordered materials, on the other hand, have no long-range order, which results in a quasicontinuous distribution of transport states with no well-defined bands. In these materials, one can distinguish only between extended and localized states. The dense bands of delocalized states are located above and below the band gap. An exponential or Gaussian tail of localized trap states extends from the delocalized bands into the band gap. The energy that separates the extended states from the localized ones is called the mobility edge. The charge-carrier mobility in the extended states above the mobility edge is much higher than that in the localized states below the mobility edge. At low carrier densities or low temperatures, all carriers reside in deep traps, meaning that the mobility will be very low. However, when the temperature is high or there are many charge carriers, the higher energetic states will be filled, and carriers will be able to move. A common approach is to

express mobility, which is dependent upon the filling of trap states in terms of the ratio of the carrier density located in extended states versus the total carrier density [18]:

$$\bar{\mu}_{e(h)} = \frac{1}{d} \int_0^d \mu_{e(h)}^0 \frac{n_{e(h)}^{\text{free}}(x)}{n_{e(h)}^{\text{free}}(x) + n_{e(h)}^{\text{trapped}}(x)} dx, \quad (7)$$

where $\mu_{e(h)}^0$ is the mobility of free electrons or holes traveling via extended states beyond the mobility edge, $n_{e(h)}^{\text{free}}$ is the density of free carriers, $n_{e(h)}^{\text{trapped}}$ is the density of trapped carriers in localized states within the exponential band tail, and d is the device thickness. Hence, if no carriers are trapped within the band gap, the mobility is constant and equal to the average mobility of carriers moving through the extended states. Otherwise, the presence of the term $n_{e(h)}^{\text{trapped}}$ will impinge a carrier dependence on the mobility $\mu_{e(h)}$, as trapping and detrapping are strongly affected by a change of operation conditions. We intend to determine exactly this carrier-dependent mobility. It is important to note that in measurements, only the spatially averaged mobility is accessible.

For this purpose, we revisit and generalize the methods of Schiefer *et al.* [22] and Albrecht *et al.* [21]. The core of their methods is Eq. (1), which has been independently established by the two research groups using different approaches. Both have in common that constant and equal gradients of quasi-Fermi-levels of electrons and holes were assumed. We follow mainly the approach of Schiefer *et al.* [22], while the one by Albrecht *et al.* [21] is discussed in the Supplemental Material [34].

We assume a solar cell with active layer thickness d and selective Ohmic contacts. Figure 2 depicts a schematic view of the energy diagram of a solar cell under illumination and an applied forward voltage $V(J)$. The majority hole contact is located at $x = 0$, and the majority electron contact at $x = d$. The transport of charges through the

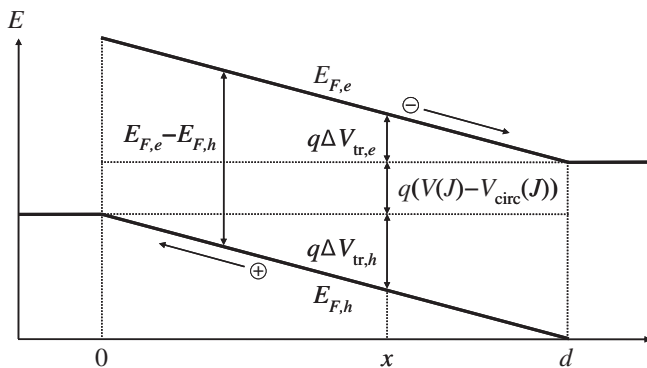


FIG. 2. Schematic sketch of the energy diagram of a solar cell with selective hole and electron contacts under illumination and forward-bias voltage (adapted from Refs. [21,22]). The majority hole contact is located at $x = 0$ and the majority electron contact at $x = d$.

photoactive layer brings about a voltage drop. At a location x in the device, it is composed of the voltage drop $\Delta V_{tr,h}$ due to hole transport from x to the hole contact and $\Delta V_{tr,e}$ due to electron transport from x to the electron contact. These voltage drops can be described in terms of the gradient of the quasi-Fermi-levels of electrons and holes $\nabla E_{F,e(h)}$, the driving force for their transport:

$$\Delta V_{tr,h}(x) + \Delta V_{tr,e}(x) = \int_0^x \nabla E_{F,h}(x') dx' + \int_x^d \nabla E_{F,e}(x') dx'. \quad (8)$$

The assumption of constant and equal gradients of the quasi-Fermi-levels $\nabla E_{F,e} = \nabla E_{F,h} = \nabla E_F$ leads to

$$\nabla E_{F,h}(x) \int_0^x dx' + \nabla E_{F,e}(x) \int_x^d dx' = \nabla E_F d = \text{const} = V_{tr}. \quad (9)$$

As can be deduced from Fig. 2, the constant gradient of the Fermi level times the thickness d equals the total voltage drop V_{tr} . $\nabla E_{F,e(h)}$ can be expressed in terms of the current, the mobility, and carrier density as

$$\nabla E_{F,e(h)} = \frac{J_{e(h)}}{\sigma_{e(h)}}. \quad (10)$$

For any x inside the photoactive layer, the total current J is the sum of the electron and hole current densities:

$$J = J_e(x) + J_h(x) = q(\mu_e(x)n_e(x) + \mu_h(x)n_h(x))\nabla E_F. \quad (11)$$

Combining Eqs. (9) and (11), we obtain

$$\mu_e(x)n_e(x) + \mu_h(x)n_h(x) = \frac{Jd}{qV_{tr}(J)}. \quad (12)$$

The transport voltage V_{tr} can be associated to a transport resistance via $V_{tr} = J R_{tr}$. This leads us to the following general relationship:

$$\mu_e(x)n_e(x) + \mu_h(x)n_h(x) = \frac{d}{qR_{tr}(J)}. \quad (13)$$

To get from here to Eq. (1), Schiefer *et al.* and Albrecht *et al.* made further simplifications already mentioned in the Introduction. Schiefer *et al.* [22] made two more assumptions: (1) the spatially averaged electron and hole current densities are equal and half the total current density $\bar{J}_e = \bar{J}_h = J/2$, and (2) the electron and hole mobilities are equal and constant $\mu_h = \mu_e = \text{const}$. Both assumptions

lead to the following simplification for the spatially averaged carrier density: $\bar{n}_h = \bar{n}_e = \bar{n}$. In Fig. S2 in the Supplemental Material [34], we demonstrate that all three currents in assumption (1) agree only at V_{OC} if both the carrier densities and mobilities are fairly balanced. Assumption (2) is a strong limitation for the method and, in general, rarely the case in disordered solar cells [35].

Albrecht *et al.* [21], in turn, made three further assumptions: (1) the electron and hole current densities are equal everywhere in the photoactive layer: $J_e(x) = J_h(x)$ so that $\mu_e(x)n_e(x) = \mu_h(x)n_h(x)$, (2) the extracted charge from the integral of the CE transient is half the sum of the electrons and holes, and (3) the electron and hole carrier densities are constant throughout the device so that $\bar{n}_{e(h)} = n_{e(h)}$. These assumptions result in an effective mobility $\bar{\mu}_{eff} = (2\mu_e\mu_h)/(\mu_e + \mu_h)$. The first assumption is generally not valid: As soon as a current flows in forward direction, the electron current density increases steadily from $J_e(0) \approx 0$ at the hole contact to $J_e(d) \approx J$ at the electron contact (see Fig. S2 in the Supplemental Material [34]). The opposite is true for the hole current density, which means that assumption (1) is wrong for $J > 0$. At V_{OC} , we have by definition $J = 0$ so that $J_e(x) = -J_h(x)$. As shown in Eq. (4), assumption (2) is valid as long as recombination and the difference between surface charges on the contacts can be neglected. Finally, assumption (3) puts a strong limitation on the method. Würfel *et al.* [1] established a different relationship using the geometrical mean of the electron and hole carrier density. However, it was also based on the additional assumption that $J_e(x) = J_h(x)$ everywhere in the bulk.

If the total carrier density \bar{n} is measured in experiment, we show in the Supplemental Material [34] that Eq. (13) can be transformed without any further presumptions into

$$\mu_{eff}(J) = \left(1 / \left(\mu \pm \Delta\mu \frac{\Delta n}{n}\right)\right)^{-1} = \frac{d}{2q\bar{n}(J)R_{tr}(J)}. \quad (14)$$

μ is the arithmetic mean of the electron and hole mobilities: $\mu(x) = (\mu_e(x) + \mu_h(x))/2$, and $\Delta\mu$ is the difference between the mobilities and the arithmetic mean: $\mu_{e(h)}(x) = \mu(x) \pm \Delta\mu(x)$. The same holds for n and Δn ; the bars denote spatial averages. The plus sign in Eq. (14) corresponds to the case where both the mobility and carrier density of one carrier type are higher than their counterparts [e.g., $\mu_e(x) > \mu_h(x)$ and $n_e(x) > n_h(x)$]. The minus sign stands for the case where the mobility and carrier density of the same carrier type show opposite behavior [e.g., $\mu_e(x) > \mu_h(x)$ and $n_e(x) < n_h(x)$]. Note that, in general, one cannot assume that because the mobility of one carrier type is higher than the other that its carrier density must be also higher, as this also depends on the density of trap states.

We already indicate above that the TPV and TPC measure the photogenerated carrier density \bar{n}_{ph} instead of \bar{n} . Instead of expressing carrier densities by their mean and differences, we divide them into an equilibrium carrier density in the dark $n_{0e(h)}$ and photogenerated carrier density $n_{ph,e(h)}$: $n_{e(h)}(x) = n_{0e(h)}(x) + n_{ph,e(h)}(x)$. The relationship between \bar{n}_{ph} and $n_{ph,e(h)}$ is given by $\bar{n}_{ph} = \frac{1}{2}(n_{ph,e} + n_{ph,h})$. Then, we can find a similar definition of μ_{eff} (see the Supplemental Material [34]):

$$\mu_{eff}(J) = \left(1 / \left(\mu + \frac{\mu(n_{0e} + n_{0h}) \pm \Delta\mu(n_e - n_h)}{(n_{ph,e} + n_{ph,h})}\right)\right)^{-1} = \frac{d}{q\bar{n}_{ph}(J)R_{tr}(J)}. \quad (15)$$

We find that in most cases the second term under the overbar in Eq. (15) can be neglected so that $\mu_{eff}(J) = \left(1/(\mu)\right)^{-1}$.

IV. DETERMINATION OF THE TRANSPORT RESISTANCE

The key to using Eqs. (14) and (15) is also being able to determine the transport resistance R_{tr} , which is caused by the transport of electrons and holes through the device. For this purpose, any method that is able to measure the series resistance as a function of voltage or current is suitable. This is because the series resistance is composed of R_{tr} and the circuit resistance R_{circ} . Prominent ways to calculate the series resistance are the comparison of the dark and light J - V curves [36], the comparison of two J - V curves at different light intensities [37], or the combination of the J - V measurement under illumination with a Suns- V_{OC} or J_{SC} - V_{OC} curve [38]. The latter two curves are pseudo- J - V curves, which are equivalent to a standard J - V curve for a solar cell that has no series resistance. In the approach by Schiefer *et al.* [22], a J_{SC} - V_{OC} curve was taken for the simulation, while the Suns- V_{OC} method was used in the measurement.

Here, we compile a J_{SC} - V_{OC} curve from the steady-state region of the TPV and TPC measurements at different bias-light intensities I_{light} . V_{OC} corresponds to the bias voltage V_{bias} [see Figs. 1(a) and 1(c)]. J_{SC} is obtained using the superposition of the short-circuit current density at 1 sun, $J_{SC}|_{1sun}$, and the current-density curve proportional to I_{light} , $-J_{SC}|_{1sun}I_{light}$ [32,39]:

$$J_{SC}(V_{OC}) = J_{SC}|_{1sun}(1 - I_{light}(V_{OC})). \quad (16)$$

$J_{SC}|_{1sun}$ is determined from the light J - V curve, while I_{light} should ideally be measured independently during the TPV and TPC measurements. Alternatively, it may also be computed from the ratio of the bias-current density J_{bias}

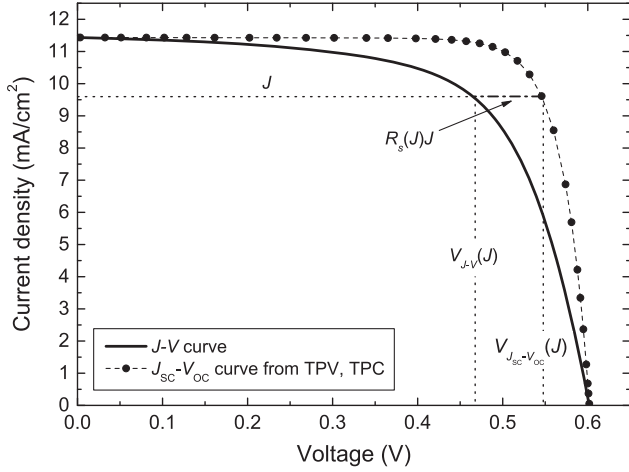


FIG. 3. Simulated J - V and J_{sc} - V_{oc} curves obtained from the steady-state part of the TPC and TPV simulations. The dotted lines indicate how the series resistance is computed from the difference of both curves.

and $J_{sc}|_{1sun}$. However, this is only valid if the relationship between J_{bias} and light intensity is linear, as is the case for the simulation shown in Fig. 1(c). Instead, the relationship is generally given by a power law $J_{bias} \propto I_{light}^\alpha$ where the exponent α has been found to vary between 0.7 and 1 depending on the photoactive material [39,40].

Figure 3 depicts the comparison of simulated J - V and J_{sc} - V_{oc} curves of a typical organic solar cell. The cell characteristics are described in the Simulation section. The J - V curve is affected by a significant amount of trapping, which manifests itself in a high series resistance (due to the relationship between carrier density and mobility) and, thus, low fill factor. The J_{sc} - V_{oc} curve, on the contrary, is impervious to this effect. As indicated by Fig. 3, the series resistance at current density J is given by the difference between the corresponding voltages of the two curves divided by J :

$$R_s(J) = \frac{V_{J_{sc}-V_{oc}}(J) - V_{J-V}(J)}{J} = R_{tr} + R_{circ}. \quad (17)$$

In order to determine R_s of a solar cell, the current at the maximum power point is chosen [38]. For our purposes, we extend the method to all current densities except $J = 0$ and $J = J_{sc}$. At the latter current, Eq. (17) suggests zero series resistance, which, of course, is not true, as at this operation point the highest current is extracted from the device. R_{circ} can be estimated from R_s at high current in forward direction, where transport resistance is minimal [22].

Even though not stated explicitly, the approach of Albrecht *et al.* [21] also relies on extracting the series resistance from a combination of the J - V and Suns- V_{oc} curves. The charge extraction under the first measurement condition, where a forward-bias voltage is applied under illumination, corresponds to the J - V measurement. The

charge extraction under the second condition, where the device is held at open circuit at a lower light intensity, corresponds to the Suns- V_{oc} measurement in this work. However, instead of subtracting two voltage points at the same current as we do, they compared two voltage points at the same measured carrier density. This is generally not valid and is discussed in the Supplemental Material [34].

V. SIMULATION

To investigate the accuracy of the investigated method, we use an open-source Shockley-Read-Hall-based [41] drift-diffusion-device model, the general-purpose photovoltaic device model (gpvdm) [30,42–45], which is adapted for this work to simulate the steady-state J - V curve, and transient photovoltage and photocurrent. The model can be downloaded from Ref. [45], along with example simulations from this paper. We then use the above method to extract the mobility from the simulated results just as one would do from experimental results. The advantage of this approach is that it enables us to compare the mobility one obtains from our proposed method to the mobility value present within the device model. The device model solves Poisson's equation between the front and back contact of the device to account for electrostatic effects,

$$\frac{d}{dx} \epsilon_0 \epsilon_r \frac{d}{dx} \varphi = q(n_f + n_t - p_f - p_t), \quad (18)$$

where ϵ_0 is the permittivity of free space, ϵ_r is the relative permittivity of the photoactive layer, φ is the electrostatic potential, and q is the elementary charge on an electron. n_f (n_t) and p_f (p_t) are the densities of free (trapped) electrons and free (trapped) holes respectively. To describe charge transport in the device, the drift-diffusion equations are solved for electrons

$$J_n = q\mu_e n_f \frac{\partial E_{LUMO}}{\partial x} + qD_n \frac{\partial n_f}{\partial x} \quad (19)$$

and for holes

$$J_p = q\mu_h p_f \frac{\partial E_{HOMO}}{\partial x} - qD_p \frac{\partial p_f}{\partial x}, \quad (20)$$

where J_n and J_p are the current densities of electrons and holes, μ_e and μ_h are the electron and hole mobilities, D_n , D_p are diffusion coefficients, and E_{LUMO} and E_{HOMO} represent the free-carrier mobility edges. For both electrons and holes, we assume an exponential distribution of trap states of form

$$\rho(E) = N \exp(E/E_u), \quad (21)$$

where ρ represents the energetic distribution of trap states, N is the maximum density of trap states, E is

TABLE I. Main simulation parameters as defined in Ref. [30]. Changes to case 1 are shown in bold.

Parameter	Unit	Case 1	Case 2	Case 3	Case 4	Case 5
Electron density on right contact	cm ⁻³	10 ²⁰	10 ²⁰	10¹⁹	10 ²⁰	2.65×10¹⁹
Hole density on left contact	cm ⁻³	10 ²⁰	10 ²⁰	10 ²⁰	10 ²⁰	5.80×10²⁰
DOS distribution		Exponential	Exponential	Exponential	Exponential	Exponential
Effective electron trap density	cm ⁻³ eV ⁻¹	0	0	0	10²⁰	3.80×10²⁰
Effective hole trap density	cm ⁻³ eV ⁻¹	0	0	0	10²⁰	1.45×10¹⁹
Characteristic energy for electron tail	meV	60	60	60	60	40
Characteristic energy for hole tail	meV	60	60	60	60	60
Free-electron mobility	cm ² /(V s)	2.48 × 10 ⁻⁰³	2.48 × 10 ⁻⁰³	2.48 × 10 ⁻⁰³	2.48 × 10 ⁻⁰³	2.48 × 10 ⁻⁰³
Free-hole mobility	cm ² /(V s)	2.48 × 10 ⁻⁰³	2.48×10⁻⁰⁴	2.48 × 10 ⁻⁰³	2.48 × 10 ⁻⁰³	2.48 × 10 ⁻⁰³
Number of traps		0	0	0	20	20
LUMO electron-capture cross section	cm ⁻²	10 ⁻²⁹	10 ⁻²⁹	10 ⁻²⁹	10⁻²⁶	2.50×10⁻²⁴
LUMO hole-capture cross section	cm ⁻²	10 ⁻²⁹	10 ⁻²⁹	10 ⁻²⁹	10⁻²⁶	1.32×10⁻²⁶
HOMO electron-capture cross section	cm ⁻²	10 ⁻²⁹	10 ⁻²⁹	10 ⁻²⁹	10⁻²⁶	4.67×10⁻³²
HOMO hole-capture cross section	cm ⁻²	10 ⁻²⁹	10 ⁻²⁹	10 ⁻²⁹	10⁻²⁶	4.86×10⁻²⁶
Effective density of free-electron states	cm ⁻³	5 × 10 ²⁰	5 × 10 ²⁰	5 × 10 ²⁰	5 × 10 ²⁰	1.28×10²¹
Effective density of free-hole states	cm ⁻³	5 × 10 ²⁰	5 × 10 ²⁰	5 × 10 ²⁰	5 × 10 ²⁰	2.86×10¹⁹

the energy, and E_u is the characteristic tail slope energy representing the degree of energetic disorder in the material system. Under each mesh point in position space, the distribution of trap states in energy space (for both electrons and holes) is divided into ten regions of width ΔE . For each of these regions, the Shockley-Read-Hall capture or escape

$$\frac{dn_t}{dt} = r_{EC} - r_{EE} - r_{HC} + r_{HE} \quad (22)$$

is solved, where n_t is the electron trap density, r_{EC} is the rate of electron capture into a trap, r_{EE} is the rate of electron escape from a trap, r_{HC} is the rate of hole capture into an electron trap, and r_{HE} is the rate of hole escape from an electron trap. Light propagation is modeled using the transfer-matrix method; for computational efficiency, the equations are projected onto a 1D finite-difference grid [46]. Some further details are given in the Supplemental Material [34].

The material parameters are taken from Ref. [30], which are obtained via calibration of the model to multiple data sets including TPV, TPC, charge extraction, and light and dark current-voltage curves (see Table I and Table SI in the Supplemental Material [34]). The parameters represent the standard set of parameters for a P3HT:PCBM organic solar cell.

We model the J - V curve at 300 K and 1 sun using the AM1.5g spectrum. For the TPV and TPC simulations, we assume a typical measurement setup with bias light, small perturbation light, and data acquisition via an oscilloscope. The bias light has the same spectrum as above, and its intensity is changed between 0 and 1.26 suns. A cw laser with wavelength 309 nm and a pulse width of 5 ns is used

for the small-signal perturbation. The ratio of laser versus bias-light intensity is adjusted in a way so that the ratio of excess photovoltage peak versus bias voltage $\Delta V/V$ is always in the range of 1%–2%. The resulting voltage transients can be almost exactly approximated by a single exponential decay function. In the case of TPV, the voltage is measured across an open circuit, and in the case of TPC, the short-circuit current is measured across a 50- Ω resistor. We simulate the entire transients using 500 evenly spaced time-domain steps. Only for the analysis of the excess carrier density [Eq. (4)], do we use a logarithmically increasing step size to reduce computational time. It is important to use a small step size as the trapping and detrapping of charge carriers happens at a much faster scale as the decay time of the laser pulse.

We simulate five different cases of an organic solar cell (see Table I for the main simulation parameters):

- (1) equal electron and hole carrier densities, equal electron and hole mobilities, and no trapping;
- (2) equal electron and hole carrier densities, much higher electron than hole mobilities, and no trapping;
- (3) much higher hole than electron carrier densities, equal electron and hole mobilities, and no trapping;
- (4) equal electron and hole carrier densities, equal electron and hole mobilities, and strong trapping;
- (5) a realistic organic solar cell whose measured characteristics have been previously simulated in Ref. [30].

Case 1 is the ideal case and serves to demonstrate the validity of the theory behind the analytical model for extracting charge-carrier mobility. As in this case the mobilities of electrons and holes are equal and no trapping occurs, the spatially averaged mobility is independent of

current. The same should happen for the one extracted from the method, as long as the condition of constant gradients of quasi-Fermi-levels are met. Cases 2–4 demonstrate step by step the resilience of the method as we move away from the case of a symmetric device with no trapping to an asymmetric device with considerable charge-carrier trapping.

Figure 3 shows the J - V and J_{SC} - V_{OC} curves of case 5. The remaining curves and the characteristic parameters V_{OC} , J_{SC} , FF, and solar-cell efficiency are included in the Supplemental Material [34]. Most interesting for our method is the difference between the J - V and J_{SC} - V_{OC} curves at the same current density, as this is proportional to the transport resistance R_{tr} according to Eq. (17). Cases 1 and 2 lead to a higher FF than for case 5, so that the difference between the J - V and J_{SC} - V_{OC} curves is smaller than seen in Fig. 3. Case 3 has a lower V_{OC} compared to cases 1 and 2 but a similar FF to cases 1 and 2. Therefore, R_{tr} for those cases is lower, and the mobility is likely to be higher than for case 5, since μ is inversely proportional to R_{tr} . For case 4, the large trapping strongly affects all J - V characteristic parameters but above all FF. As a result, it shows a very high transport resistance and, thus, a very low mobility.

VI. RESULTS AND DISCUSSION

At the core of the investigated method is Eq. (15), which states that the effective mobility is inversely proportional to the average carrier density and the transport resistance. Hence, the accuracy of the effective mobility crucially depends on how accurately we can determine these two parameters. The assumptions made in the derivation of Eq. (15) certainly play a role also. We notice that the determination of the carrier density and transport resistance have the highest impact on the shape of the extracted mobility. The spatial variation of the quasi-Fermi-levels, however, plays a minor role, as it is practically constant at V_{OC} and varies only gradually at J_{SC} . We choose to outline its contribution in the Supplemental Material (see Sec. III. C in the Supplemental Material [34]).

A. Extraction of the excess carrier density

We first investigate the extraction of the excess carrier density Δn_{TPC} from the TPC signal. As we delineate in the theory part, Δn_{TPC} can be computed from the area under the current transient. We see that if the difference between carrier densities on the contacts, surface recombination, and trapping are neglected, Δn_{TPC} is proportional to this area. In Fig. 4, the excess carrier density calculated from the TPC simulation Δn_{TPC} is compared to the components of the right-hand side of Eq. (6) for case 1. Instead of plotting the excess carrier densities against J_{bias} , we convert the latter to

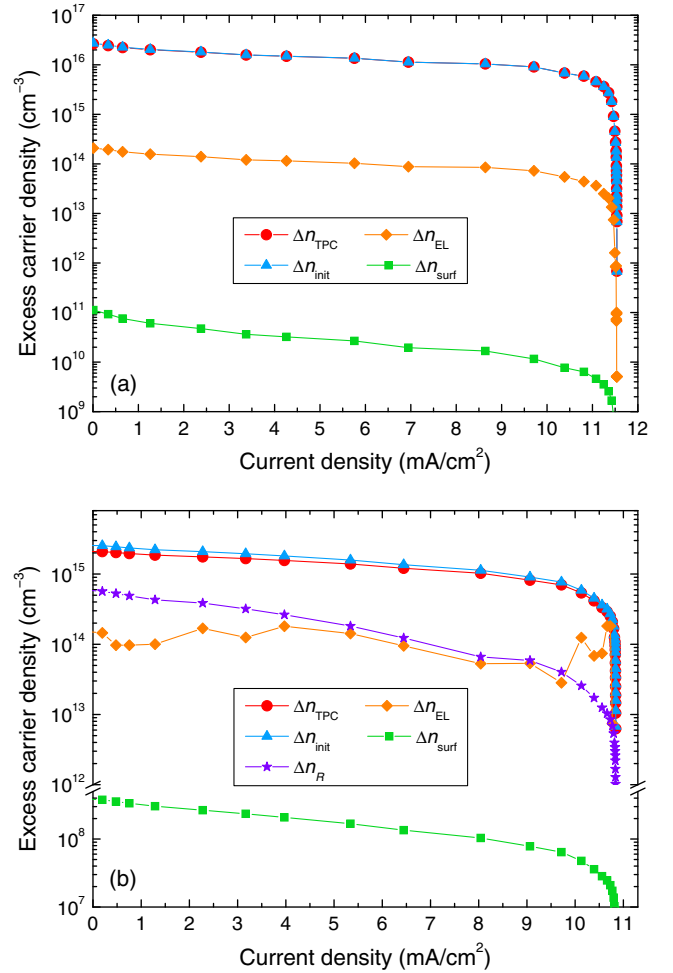


FIG. 4. (a) Excess carrier density as a function of current density for case 1 (equal carrier densities, equal free-carrier mobilities, no trapping). (b) Excess carrier density as a function of current density for case 4 (equal carrier densities, equal free-carrier mobilities, and trapping). Δn_{TPC} denotes the excess carrier density obtained from the area under the current transient. The other excess carrier densities correspond to the components of the right-hand side of Eq. (6): $\Delta n_{init} = 1/2 (\Delta n_{e,init} + \Delta n_{h,init})$ is the excess carrier density present right after the small-signal light pulse is switched off. Δn_{EL} represents the change in the difference between the carrier densities on the contacts. Δn_{surf} and Δn_R stand for the excess carrier densities lost due to surface and bulk recombination, respectively.

J_{SC} (V_{OC}) using Eq. (16) to better compare it to later results. In Fig. 4, a current density of 0 then corresponds to V_{OC} and the asymptotic limit at high current densities to J_{SC} .

For case 1, it can be seen that excess carrier densities are fairly constant throughout the current-density range but drop rapidly towards J_{SC} . Δn_{EL} is around 2 orders of magnitude lower than Δn_{init} for almost the entire current-density range. The number of carriers lost to surface recombination is negligible, since Δn_{surf} is more than

5 orders of magnitude lower than Δn_{init} . As trapping is suppressed, bulk recombination does not influence the result. Consequently, we can say that Δn_{TPC} indeed equals the initial excess carrier density at every current density for the case of an ideal solar cell. A similar scenario is found for cases 2 and 3 (see the Supplemental Material [34]).

In Fig. 4(b), the recombination via trap states is added (case 4). The absolute level of Δn_{init} is smaller by about 1 order of magnitude compared to the case without trapping. This is rooted in the fact that the intensity of the small-signal light pulse has to be lowered so that the ratio of the peak excess voltage to the steady-state voltage $\Delta V/V$ is below 2%. As explained earlier, this is to ensure that the excess voltage decays monoexponentially.

The inclusion of trapping leads to a smaller difference between Δn_{init} and Δn_{EL} of about 1 order of magnitude and a much lower Δn_{surf} compared to case 1. However, the bulk recombination via trap levels now plays a major role. At V_{OC} , the bulk recombination is the strongest, where Δn_R is only a factor of 2 lower than Δn_{init} . For higher current densities, Δn_R decreases much more strongly than Δn_{init} . According to Eq. (6), Δn_{TPC} is, thus, slightly lower than Δn_{init} because of the impact of Δn_R . Nevertheless, we can state that Δn_{TPC} is still a good measure of Δn_{init} .

Case 5 contains the effect of very unbalanced charge-carrier densities, unbalanced mobilities, and trapping. Despite this, Δn_{TPC} is only slightly lower than Δn_{init} , since the former is decreased by recombination and the change in carrier density on the contacts because of trapping and detrapping (see the Supplemental Material [34]). These findings show that the area under the small-signal current transient is indeed a good measure of the initial excess carrier density despite very unbalanced carrier properties or large trapping.

We now compare the average carrier density obtained from the TPV and TPC simulation, $\bar{n}_{\text{TPV,TPC}}$, with the theoretical \bar{n} extracted at each point of the J - V and J_{SC} - V_{OC} curves. Figure 5(a) depicts the carrier density as a function of bias-light intensity (upper x axis) and bias voltage V (lower x axis) of case 1. Here, we deal with equal electron and hole carrier densities and equal mobilities. The triangles show the theoretical carrier density \bar{n} extracted from the steady-state part of the TPV signal. This carrier density corresponds to the total carrier density at the bias-light intensity or, alternatively, bias voltage. The diamonds stand for the photogenerated carrier density \bar{n}_{ph} , which is obtained from the former by subtracting the carrier density in the dark. $\bar{n}_{\text{TPV,TPC}}$ is the carrier density deduced from the combination of the TPV and TPC simulations by means of the differential capacitance method.

For very small light intensities, \bar{n} remains nearly constant and equals the carrier density in the dark, since \bar{n}_{ph} is minuscule in comparison. Only when the light intensity increases considerably, \bar{n}_{ph} augments and approaches \bar{n} . In the description of the differential capacitance method

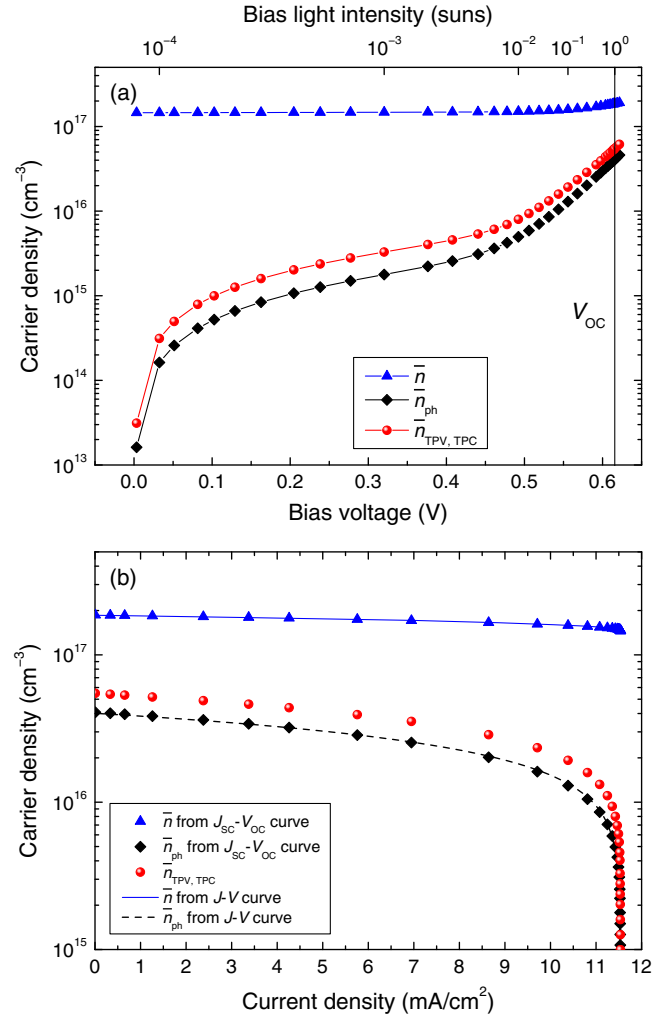


FIG. 5. (a) Carrier densities as a function of bias-light intensity (upper x axis) and bias voltage (lower x axis) of the TPV simulation for case 1. The triangles and diamonds stand for the average carrier density \bar{n} and the photoinduced carrier density \bar{n}_{ph} , respectively, determined from the steady-state part of the TPV signal. The circles correspond to the carrier density $\bar{n}_{\text{TPV,TPC}}$ obtained from the differential capacitance method. (b) Carrier densities as a function of current density for case 1. The symbols stand for the same parameters as in part (a). The bias intensity is converted to current density via Eq. (16). In addition, \bar{n} and \bar{n}_{ph} as determined from the J - V curve are shown (continuous and dashed line, respectively).

above, we imply that $\bar{n}_{\text{TPV,TPC}}(V)$ includes only the photo-generated carrier density. This is corroborated by the findings of Fig. 5(a), as $\bar{n}_{\text{TPV,TPC}}(V)$ follows the shape of \bar{n}_{ph} . Albeit that, $\bar{n}_{\text{TPV,TPC}}(V)$ overestimates \bar{n}_{ph} . The gap closes only for light intensities above 0.5 suns, or in terms of voltage, close to $V_{\text{OC}} = 0.646$ V [vertical line in Fig. 5(a)].

The representation of Fig. 5(a) is very suitable to focus on the small intensity range of the TPV measurement due to the exponential relationship between intensity and V_{OC} . Yet, the mobility is defined as a function of current density

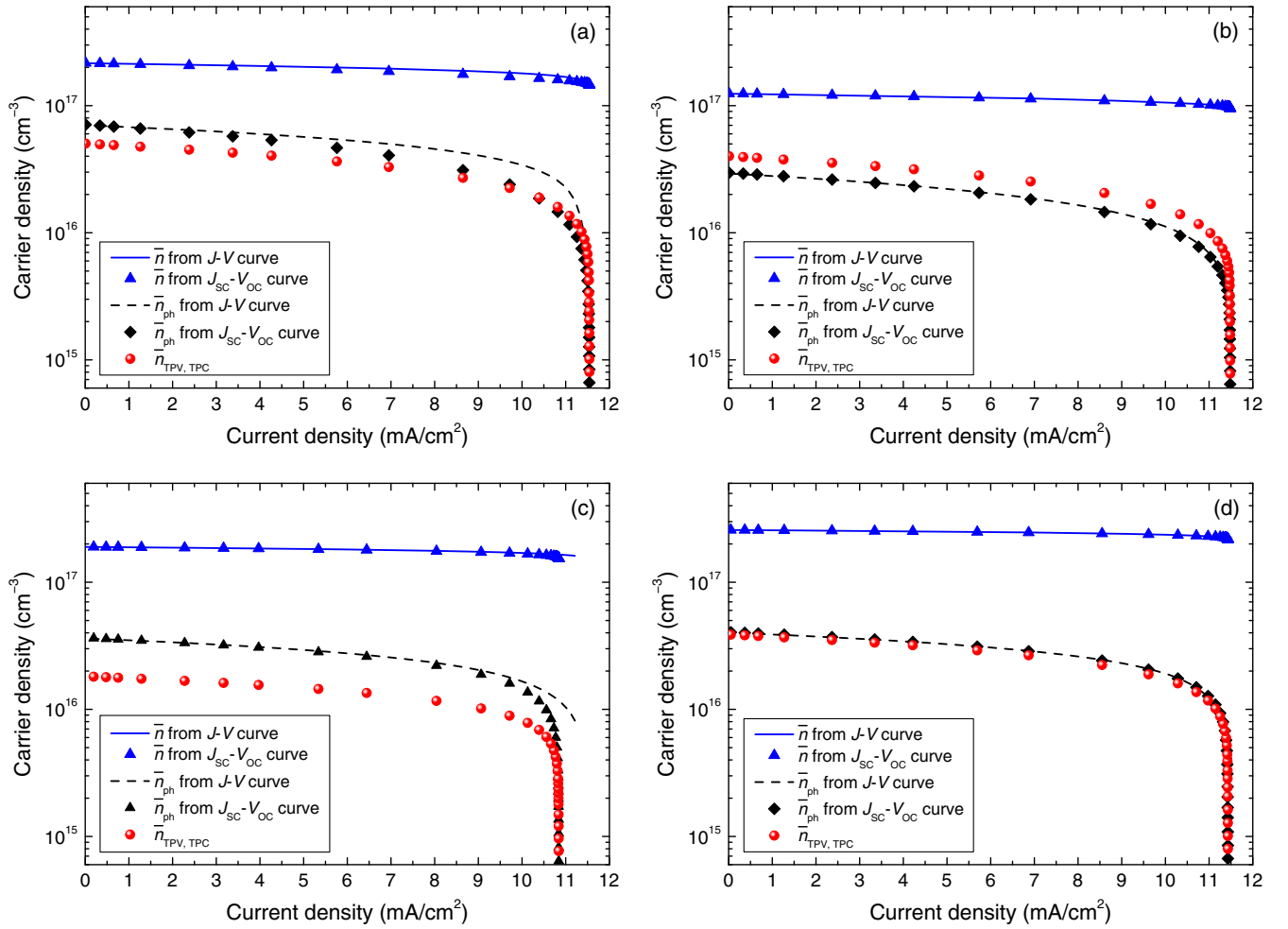


FIG. 6. Spatially averaged carrier densities as a function of current density for cases 2–5. (a) Case 2, (b) case 3, (c) case 4, and (d) case 5. The continuous line corresponds to the average carrier density \bar{n} obtained from the J - V curve. Triangles stand for \bar{n} deduced from the J_{SC} - V_{OC} curve. The dashed line represents the photoinduced carrier density \bar{n}_{ph} from the J - V curve. The carrier density obtained from TPV and TPC $\bar{n}_{TPV,TPC}$ is plotted with circles.

in Eq. (15). For this purpose, we convert the bias-light intensity to current densities using the superposition principle as described by Eq. (16). Instead of plotting \bar{n} versus the bias-light intensity or bias voltage as in Fig. 5(a), we now plot it versus the corresponding current density J_{SC} . Figure 5(b) depicts the so-deduced \bar{n} as a function of J_{SC} together with \bar{n} computed at each point of the J - V curve. By converting from intensity to current densities, the trend in the curves is reversed, as V_{OC} is now situated on the left-hand side of Fig. 5(b) (at zero current density). Instead of the small intensity range, the current-density range corresponding to V_{OC} and the maximum power point is now stretched out.

The carrier densities \bar{n} obtained from the J - V and J_{SC} - V_{OC} curves stay nearly constant for increasing current density and fall off only slightly when approaching J_{SC} . Both curves match perfectly over the entire current range. The carrier densities \bar{n}_{ph} deduced from the J - V curve and

J_{SC} - V_{OC} curves are also in perfect agreement but lie clearly below and exhibit a strong decrease for increasing current densities. As already seen in Fig. 5(a), $\bar{n}_{TPV,TPC}$ follows the same shape as \bar{n}_{ph} but with slightly higher values.

We now shift the focus to Fig. 6, where we add deviations from the ideal case 1 in the form of unequal carrier densities, unbalanced mobilities, or trapping. Figure 6 displays the same meaning for the lines and symbols as in Fig. 5(b). On the left-hand side of Fig. 6, the cases 2 and 4 with equal electron and hole carrier densities are shown. The right-hand side depicts cases 3 and 5 with unbalanced carrier densities. The corresponding figures of the carrier densities as a function of bias voltage are included in the Supplemental Material [34].

For cases 2–5, it can be seen that \bar{n} obtained from the current-voltage curves displays the same behavior as case 1: Both carrier density curves perfectly overlap and are

much higher than \bar{n}_{ph} . The perfect agreement between both \bar{n}_{ph} curves, on the contrary, is only true for the cases with equal mobilities (cases 3 and 5). For the cases with unbalanced mobilities, the curves coincide only for low current densities. The strongest difference between all cases and the most important one regarding the determination of the mobility is the offset between \bar{n}_{ph} from the $J_{\text{SC}}-V_{\text{OC}}$ curve and $\bar{n}_{\text{TPV,TPC}}$.

Now let us turn to each case in detail. For case 2, the hole mobility is lowered by 1 order of magnitude. This has the effect that $\bar{n}_{\text{TPV,TPC}}$ lies about 20% below \bar{n}_{ph} for the main current-density range. For case 3, the electron carrier density on the left contact is lowered by 1 order of magnitude compared to case 1 [Fig. 6(b)]. In practice, this means that the left contact is changed to a less Ohmic contact. As a result, all carrier densities are lowered by about 30% over the entire current-density range compared to case 1. Furthermore, $\bar{n}_{\text{TPV,TPC}}$ overestimates \bar{n}_{ph} by about 40% for the entire current-density range.

Figure 6(c) plots the carrier densities for case 4, where trapping via electron and hole traps is added in comparison to case 1. The trapping does not impact on the total carrier density \bar{n} and \bar{n}_{ph} determined from the $J_{\text{SC}}-V_{\text{OC}}$ curve. However, it causes a much stronger decrease of $\bar{n}_{\text{TPV,TPC}}$ than for cases 1 and 2. Thus, this decrease is clearly related to trapping, whose impact is expected to be more severe for higher light intensities, which translate to lower current densities via the superposition principle of Eq. (16). The simulation of the excess densities in Fig. 4(b) indeed unearths that Δn_{TPC} is slightly lower than Δn_{init} due to trapping.

Finally, case 5 incorporates all deviations from case 1 into one [Fig. 6(d)]. Regarding $\bar{n}_{\text{TPV,TPC}}$, two opposing trends come into play: Unbalanced mobilities and, above all, trapping entail that $\bar{n}_{\text{TPV,TPC}}$ is lowered compared to \bar{n}_{ph} , while unequal carrier densities at the contacts have the opposite effect. In sum, these affects cancel each other out, so that $\bar{n}_{\text{TPV,TPC}}$ matches \bar{n}_{ph} .

B. Determination of transport resistance

In Fig. 7, we plot R_{tr} as a function of current density for all cases. R_{tr} is obtained from the difference between the $J-V$ and $J_{\text{SC}}-V_{\text{OC}}$ curves [Eq. (17)]. For all cases, R_{tr} exhibits an increase near V_{OC} and a sharp peak near J_{SC} . The increase near V_{OC} stems from the fact that the current density becomes very small. At V_{OC} itself, R_{tr} is not defined owing to the definition of Eq. (17). The sharp peak at J_{SC} is rooted in the fact that for voltages below the maximum power point, the voltage difference between the $J-V$ and $J_{\text{SC}}-V_{\text{OC}}$ curves increases strongly, while the current density remains fairly constant. The curve suggests that R_{tr} is close to zero at J_{SC} ; however, this originates from the particular definition of the series resistance as a function of current density [Eq. (17)]. Converse to the peaked R_{tr} observed in Fig. 7, Eq. (13) predicts that R_{tr} should vary

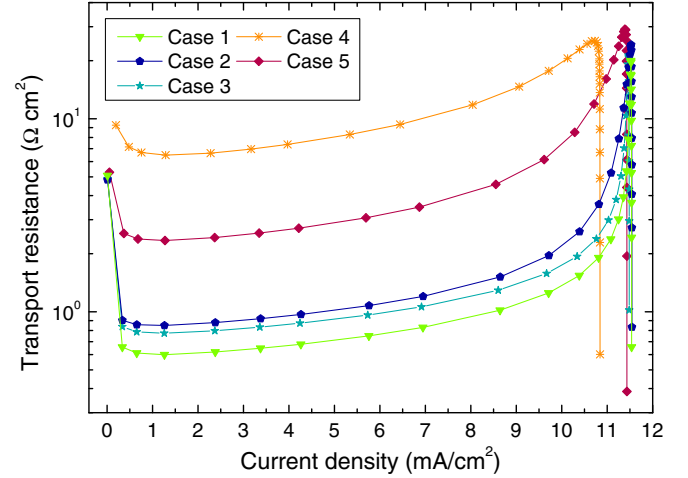


FIG. 7. Transport resistance R_{tr} as a function of current density for all cases.

only slightly with current density. This is due to the fact that \bar{n} is nearly constant except for a slight decrease towards J_{SC} [Fig. 5(b)]. As a consequence, since $\bar{\mu}_{\text{TPV,TPC}}$ is inversely proportional to R_{tr} , the features near V_{OC} and J_{SC} will be directly imprinted on $\bar{\mu}_{\text{TPV,TPC}}$ via Eq. (15).

In Sec. IV, we assume that the transport resistance dominates the series resistance. In our simulations, a contact resistance of $2.34 \Omega \text{ cm}^2$ is assumed; see the Supplemental Material, Table SI [34]. This contact resistance is taken from the measurement of a typical organic solar cell (case 5) [30]. Only for cases 1 and 3 (no trapping), R_{tr} is as low as the contact resistance for low current densities. Case 5 exhibits R_{tr} as low as $2.5 \Omega \text{ cm}^2$ for very low current densities. For case 4, which includes trapping, the lowest R_{tr} is about $7 \Omega \text{ cm}^2$. For current densities close to J_{SC} , the transport resistance increases strongly and reaches values of $15\text{--}25 \Omega \text{ cm}^2$ for all cases. Schiefer *et al.* [22] measured the circuit and transport resistances of an organic solar cell with P3HT:PCBM as active layer using the combination of $J-V$ and Suns- V_{OC} measurements. They found a circuit resistance of $2 \Omega \text{ cm}^2$, while the transport resistance varied with the current density between 6 and $23 \Omega \text{ cm}^2$ from V_{OC} to J_{SC} . It is clear from these examples that the transport resistance is comparable to the circuit resistance for solar cells for current densities below J_{SC} and devices without trapping. When trapping occurs or the current densities are close to J_{SC} , the series resistance is dominated by the transport resistance.

C. Determination of mobility

In Fig. 8, the mobility is depicted as a function of current density for all cases. For cases with equal electron and hole carrier densities at the contacts, $\bar{\mu}$ represents the spatially averaged mobility as defined in Eq. (7). For cases with unbalanced carrier densities, the spatially averaged

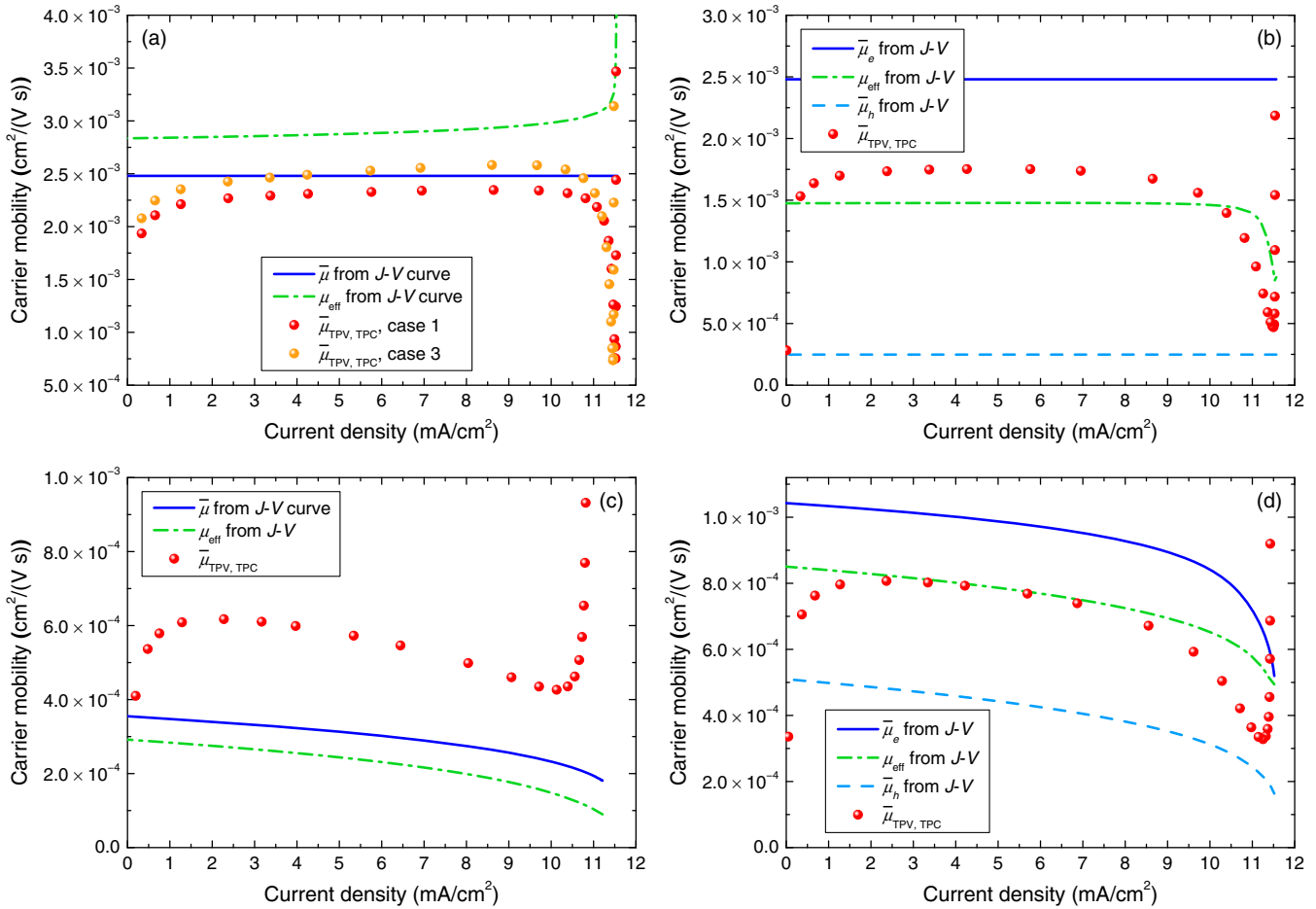


FIG. 8. Spatially averaged mobilities as a function of current density. (a) Cases 1 and 3, (b) case 2, (c) case 4, and (d) case 5. The left panel shows the cases with equal electron and hole mobilities. Here, the continuous line corresponds to the average mobility $\bar{\mu}$ as defined in Eq. (7), which is determined at each point of the J - V curve. The right panel depicts the cases with unbalanced mobilities. Here, the continuous and dashed lines are the average electron and hole mobilities $\bar{\mu}_e$ and $\bar{\mu}_h$, respectively. The dash-dotted green line corresponds to the effective mobility μ_{eff} as defined in Eq. (15). In all graphs, the mobility determined from the investigated method $\bar{\mu}_{\text{TPV,TPC}}$ is plotted with circles.

mobilities $\bar{\mu}_{e,h}$ of electrons and holes are shown separately. We include only $\bar{\mu}$ and $\bar{\mu}_{e,h}$ determined at each point of the J - V curve, as they generally agree very well with the one from the $J_{\text{SC}}-V_{\text{OC}}$ curve. μ_{eff} is the effective mobility as defined in the center of Eq. (15), that is, the theoretical mobility that can be extracted by the investigated method. $\bar{\mu}_{\text{TPV,TPC}}$ stands for the mobility determined from the right-hand side of Eq. (15); this is the mobility that is measured in experiment.

The first thing that comes to our attention is that $\bar{\mu}_{\text{TPV,TPC}}$ has a strong current-density dependence near V_{OC} and J_{SC} , a fact that is observed for all cases. The current dependences are exactly inverse to the one observed for the transport resistance in Fig. 7. This demonstrates that $\bar{\mu}_{\text{TPV,TPC}}$ cannot be determined near V_{OC} and J_{SC} due to the limitation of extracting the transport resistance.

Figure 8(a) exhibits cases 1 and 3 with equal electron and hole mobilities. The theoretical mobility, therefore, equals

the constant, predefined mobility of free carriers shown as a blue line. The theoretical μ_{eff} predicts a slightly higher mobility over almost the entire current range before experiencing a sharp increase at J_{SC} . Apart from the regions near V_{OC} and J_{SC} , $\bar{\mu}_{\text{TPV,TPC}}$ is in good accordance with the theoretical one for both cases. The slightly lower mobilities as μ_{eff} can be explained by the fact that for both cases, $\bar{n}_{\text{TPV,TPC}}$ slightly overestimates \bar{n}_{ph} [Figs. 5(b) and 6(b)]. The differences of μ_{eff} and $\bar{\mu}_{\text{TPV,TPC}}$ at J_{SC} stems from the strong impact of the curvature of the transport resistance.

Figure 8(b) depicts case 2, where the hole mobility is lowered by 1 order of magnitude compared to case 1. Here, the theoretical mobilities of electrons and holes also equal the constant, predefined mobilities of the free electron and holes. For the main current-density range, $\bar{\mu}_{\text{TPV,TPC}}$ is nearly flat and very close to μ_{eff} . It is slightly higher than the arithmetic average of $1.4 \times 10^{-4} \text{ cm}^2/(\text{V s})$ and clearly higher than the geometric average of $7.8 \times 10^{-4} \text{ cm}^2/(\text{V s})$.

As $\bar{n}_{\text{TPV,TPC}}$ slightly underestimates \bar{n}_{ph} [Fig. 6(a)], $\bar{\mu}_{\text{TPV,TPC}}$ is slightly higher than μ_{eff} .

Now we wish to discuss the impact of trapping on the mobility. For balanced carrier densities and mobilities, the effect of trapping can be best appreciated by comparing case 1 and case 4 in the left panel of Fig. 8. There are two changes that affect both the theoretical mobility $\bar{\mu}$ and $\bar{\mu}_{\text{TPV,TPC}}$: First, the carriers become less mobile by about 1 order of magnitude. Second, the mobility becomes dependent on current density with a negative slope. The first change is rooted in the fact that the trapped carrier density exceeds the free-carrier density by more than 1 order of magnitude (see Fig. S6(a) in the Supplemental Material [34]). This strongly decreases the ratio of free- to total carrier density and, therefore, $\bar{\mu}$ [Eq. (7)]. The second change stems from the fact that trapping is the strongest at J_{SC} and diminishes with decreasing current density (Fig. S6(b) in the Supplemental Material [34]). Even though μ_{eff} is very close to $\bar{\mu}$, $\bar{\mu}_{\text{TPV,TPC}}$ is higher than $\bar{\mu}$ by about a factor of 2 in the main current-density range. This is a direct cause of the fact that $\bar{n}_{\text{TPV,TPC}}$ strongly underestimates \bar{n} .

Now coming to the last case, Fig. 8(d) plots the results for a typical organic solar cell that combines all the influences of cases 2–4 into one. On the one hand, μ_{eff} and $\bar{\mu}_{\text{TPV,TPC}}$ exhibit the same current-density dependence as observed in Fig. 8(c). On the other hand, the vertical position of $\bar{\mu}_{\text{TPV,TPC}}$ is due to the combined impact of the unbalanced mobilities [Fig. 8(b)] and trapping [Fig. 8(c)]. Hence, owing to the fact that $\bar{n}_{\text{TPV,TPC}}$ agrees well with \bar{n}_{ph} , $\bar{\mu}_{\text{TPV,TPC}}$ is in good accordance with μ_{eff} in the main current-density range.

In the Supplemental Material [34], we add simulation of further cases. They are variations of cases 2 and 3 for which we increase the unbalance between mobilities and carrier densities. In the variations of case 2 (cases 2b and c), we decrease the hole mobility by 2 and 4 orders of magnitude, respectively, compared to the electron mobility. In the variations of case 3 (cases 3b and c), we reduce the electron charge on the right contact to 10^{18} and 10^{10} cm^{-3} , respectively, so that the ratio of hole to electron charge on the contacts is increased to 2 and 10 orders of magnitudes, respectively. In many thin-film solar cells, highly unbalanced mobilities and charge-carrier densities are a stark reality, for example, caused by a very poor electron-selective contact. Furthermore, many organic materials suffer from a much lower electron than hole mobility [35]. When the hole mobility is decreased by 2 orders of magnitude, $\bar{\mu}_{\text{TPV,TPC}}$ is fairly constant and agrees well with μ_{eff} for the main current-density range (case 2b). Even for a further decrease of hole mobility, a good agreement between $\bar{\mu}_{\text{TPV,TPC}}$ and μ_{eff} is found for lower current densities (case 2c). For larger current densities, μ_{eff} predicts a much lower mobility as determined by $\bar{\mu}_{\text{TPV,TPC}}$. The mobilities are much closer to μ_{eff} than to $\sqrt{\bar{\mu}_e \bar{\mu}_h}$, in contrast to what has been postulated in

Refs. [1,22]. For the variation of case 3, the following results are obtained: For an electron charge on the right contact to 10^{18} cm^{-3} , $\bar{\mu}_{\text{TPV,TPC}}$ exhibits a very similar agreement as that shown for the two cases in Fig. 8(a). When the electron charge is further decreased to 10^{10} cm^{-3} , however, $\bar{\mu}_{\text{TPV,TPC}}$ becomes strongly dependent on current density and agrees only with the theoretical mobility in a small-current-density range. Nevertheless, $\bar{\mu}_{\text{TPV,TPC}}$ determined at mid-current densities remains a good estimate of the theoretical mobility.

VII. CONCLUSIONS

A method previously proposed by Albrecht *et al.* and Schiefer *et al.* that is capable of determining the charge-carrier mobility in disordered thin-film solar cells is revisited and generalized. Revising the theory unveils that only an effective mobility can be determined, which, in general, is composed of a mix of mobility and carrier density terms. This mix depends on the exact nature of the carrier density measured by the method, that is, the total carrier density or the photoinduced one. Drift-diffusion simulation of organic solar cells shows that in the case of equal mobilities and carrier densities, the extracted mobility is in excellent agreement with the theoretical one. In the case of unequal electron and hole mobilities, the techniques determine a mobility close to μ_{eff} . In the case of unequal carrier densities up to a ratio of 2 orders of magnitude, the mobility agrees very well with the theoretical one. When trapping is present in the device, the method is able to measure the trapping-induced current-density dependence of the mobility. The accuracy of determining the mobility depends inversely on the one of the experimentally determined average carrier density.

However, the accurate extraction of mobility is restricted to current-density ranges away from V_{OC} and J_{SC} . Near V_{OC} and J_{SC} , the limitation is rooted in the fact that the transport resistance cannot be correctly determined. It is important to add that this can be circumvented for V_{OC} if the transport resistance is extracted from the J - V and J_{SC} - V_{OC} curves measured at considerably higher intensities than 1 sun. Then, V_{OC} at 1 sun will correspond to a point on the higher-intensity J - V curve, which has the same voltage but a nonzero current. The intensity should be chosen in a manner so that the 1-sun- V_{OC} point moves to the flatter part of the mobility versus the current-density curve.

-
- [1] U. Würfel, D. Neher, A. Spies, and S. Albrecht, Impact of charge transport on current-voltage characteristics and power-conversion efficiency of organic solar cells, *Nat. Commun.* **6**, 6951 (2015).
 - [2] G. Li, V. Shrotriya, J. Huang, Y. Yao, T. Moriarty, K. Emery, and Y. Yang, High-efficiency solution processable polymer

- photovoltaic cells by self-organization of polymer blends, *Nat. Mater.* **4**, 864 (2005).
- [3] O. J. Weiß, R. K. Krause, and A. Hunze, Hole mobility of 1-NaphDATA, *J. Appl. Phys.* **103**, 043709 (2008).
- [4] J. C. Blakesley, F. A. Castro, W. Kylberg, G. F. A. Dibb, C. Arantes, R. Valaski, M. Cremona, J. S. Kim, and J.-S. Kim, Towards reliable charge-mobility benchmark measurements for organic semiconductors, *Org. Electron.* **15**, 1263 (2014).
- [5] C. Tanase, E. J. Meijer, P. W. M. Blom, and D. M. de Leeuw, Unification of the Hole Transport in Polymeric Field-Effect Transistors and Light-Emitting Diodes, *Phys. Rev. Lett.* **91**, 216601 (2003).
- [6] N. I. Craciun, J. J. Brondijk, and P. W. M. Blom, Diffusion-enhanced hole transport in thin polymer light-emitting diodes, *Phys. Rev. B* **77**, 035206 (2008).
- [7] C. G. Shuttle, R. Hamilton, J. Nelson, B. C. O'Regan, and J. R. Durrant, Measurement of charge-density dependence of carrier mobility in an organic semiconductor blend, *Adv. Funct. Mater.* **20**, 698 (2010).
- [8] J. J. Brondijk, F. Maddalena, K. Asadi, H. J. van Leijen, M. Heeney, P. W. M. Blom, and D. M. de Leeuw, Carrier-density dependence of the hole mobility in doped and undoped regioregular poly(3-hexylthiophene), *Phys. Status Solidi B* **249**, 138 (2012).
- [9] W. F. Pasveer, J. Cottaar, C. Tanase, R. Coehoorn, P. A. Bobbert, P. W. M. Blom, D. M. de Leeuw, and M. A. J. Michels, Unified Description of Charge-Carrier Mobilities in Disordered Semiconducting Polymers, *Phys. Rev. Lett.* **94**, 206601 (2005).
- [10] R. A. Street, K. W. Song, J. E. Northrup, and S. Cowan, Photoconductivity measurements of the electronic structure of organic solar cells, *Phys. Rev. B* **83**, 165207 (2011).
- [11] W. C. Germs, J. J. M. van der Holst, S. L. M. van Mensfoort, P. A. Bobbert, and R. Coehoorn, Modeling of the transient mobility in disordered organic semiconductors with a Gaussian density of states, *Phys. Rev. B* **84**, 165210 (2011).
- [12] J. C. Scott, S. Ramos, and G. G. Malliaras, Transient space-charge-limited current measurements of mobility in a luminescent polymer, *J. Imaging Sci. Technol.* **43**, 233 (1999).
- [13] W. E. Spear, The study of transport and related properties of amorphous silicon by transient experiments, *J. Non-Cryst. Solids* **59**, 1 (1983).
- [14] A. Many and G. Rakavy, Theory of transient space-charge-limited currents in solids in the presence of trapping, *Phys. Rev.* **126**, 1980 (1962).
- [15] G. Juska, K. Arlauskas, M. Viliunas, and J. Kocka, Extraction Current Transients: New Method of Study of Charge Transport in Microcrystalline Silicon, *Phys. Rev. Lett.* **84**, 4946 (2000).
- [16] T. Esward, S. Knox, H. Jones, P. Brewer, C. Murphy, L. Wright, and J. Williams, A metrology perspective on the dark injection transient current method for charge mobility determination in organic semiconductors, *J. Appl. Phys.* **109**, 093707 (2011).
- [17] E. Knapp and B. Ruhstaller, The role of shallow traps in dynamic characterization of organic semiconductor devices, *J. Appl. Phys.* **112**, 024519 (2012).
- [18] R. Hanfland, M. A. Fischer, W. Büttling, U. Würfel, and R. C. I. MacKenzie, The physical meaning of charge extraction by linearly increasing voltage transients from organic solar cells, *Appl. Phys. Lett.* **103**, 063904 (2013).
- [19] T. Kirchartz, W. Gong, S. A. Hawks, T. Agostinelli, R. C. I. MacKenzie, Y. Yang, and J. Nelson, Sensitivity of the Mott-Schottky analysis in organic solar cells, *J. Phys. Chem. C* **116**, 7672 (2012).
- [20] L. M. Peter, N. W. Duffy, R. L. Wang, and K. G. U. Wijayantha, Transport and interfacial transfer of electrons in dye-sensitized nanocrystalline solar cells, *J. Electroanal. Chem.* **524–525**, 127 (2002).
- [21] S. Albrecht, J. R. Tumbleston, S. Janietz, I. Dumsch, S. Allard, U. Scherf, H. Ade, and D. Neher, Quantifying charge extraction in organic solar cells: The case of fluorinated PCPDTBT, *J. Phys. Chem. Lett.* **5**, 1131 (2014).
- [22] S. Schiefer, B. Zimmermann, and U. Würfel, Determination of the intrinsic and the injection dependent charge carrier density in organic solar cells using the Suns- V_{OC} method, *J. Appl. Phys.* **115**, 044506 (2014).
- [23] C. G. Shuttle, B. O'Regan, A. M. Ballantyne, J. Nelson, D. D. C. Bradley, J. de Mello, and J. R. Durrant, Experimental determination of the rate law for charge carrier decay in a polythiophene: Fullerene solar cell, *Appl. Phys. Lett.* **92**, 093311 (2008).
- [24] D. K. Schroder, *Semiconductor Material and Device Characterization* (John Wiley & Sons, New York, 1990).
- [25] B. C. O'Regan, S. Scully, A. C. Mayer, E. Palomares, and J. Durrant, The effect of Al_2O_3 barrier layers in TiO_2 /Dye/CuSCN photovoltaic cells explored by recombination and DOS characterization using transient photovoltage measurements, *J. Phys. Chem. B* **109**, 4616 (2005).
- [26] R. Hamilton, C. G. Shuttle, B. C. O'Regan, T. C. Hammant, J. Nelson, and J. R. Durrant, Recombination in annealed and nonannealed polythiophene/fullerene solar cells: Transient photovoltage studies versus numerical modeling, *J. Phys. Chem. Lett.* **1**, 1432 (2010).
- [27] A. Maurano *et al.*, Recombination dynamics as a key determinant of open circuit voltage in organic bulk heterojunction solar cells: A comparison of four different donor polymers, *Adv. Mater.* **22**, 4987 (2010).
- [28] C. R. McNeill, I. Hwang, and N. C. Greenham, Photocurrent transients in all-polymer solar cells: Trapping and detrapping effects, *J. Appl. Phys.* **106**, 024507 (2009).
- [29] Z. Li, F. Gao, N. C. Greenham, and C. R. McNeill, Comparison of the operation of polymer/fullerene, polymer/polymer, and polymer/nanocrystal solar cells: A transient photocurrent and photovoltage study, *Adv. Funct. Mater.* **21**, 1419 (2011).
- [30] R. C. I. MacKenzie, C. G. Shuttle, M. L. Chabiny, and J. Nelson, Extracting microscopic device parameters from transient photocurrent measurements of P3HT:PCBM solar cells, *Adv. Energy Mater.* **2**, 662 (2012).
- [31] A. Maurano, C. G. Shuttle, R. Hamilton, A. M. Ballantyne, J. Nelson, W. Zhang, M. Heeney, and J. R. Durrant, Transient optoelectronic analysis of charge carrier losses in a selenophene/fullerene blend solar cell, *J. Phys. Chem. C* **115**, 5947 (2011).
- [32] R. A. Sinton and A. Cuevas, A quasi-steady-state open-circuit voltage method for solar cell characterization,

- in *Proceedings of the 16th European Photovoltaic Solar Energy Conference, Glasgow, UK, 2000* (2000), p. 1152.
- [33] S. A. Hawks, B. Y. Finck, and B. J. Schwartz, Theory of Current Transients in Planar Semiconductor Devices: Insights and Applications to Organic Solar Cells, *Phys. Rev. Applied* **3**, 044014 (2015).
- [34] See Supplemental Material at <http://link.aps.org/supplemental/10.1103/PhysRevApplied.9.034020> for further theoretical work, simulations, parameters and figures of our investigation.
- [35] M. Soldera, K. Taretto, and T. Kirchartz, Comparison of device models for organic solar cells: Band-to-band vs. tail states recombination, *Phys. Status Solidi A* **209**, 207 (2012).
- [36] A. G. Aberle, S. R. Wenham, and M. A. Green, A new method for accurate measurements of the lumped series resistance of solar cells, in *Proceedings of the 23rd IEEE Photovoltaic Specialists Conference, Louisville, KY, 1993* (IEEE New York, 1993), p. 133.
- [37] P. P. Altermatt, G. Heiser, A. G. Aberle, A. Wang, J. Zhao, S. J. Robinson, S. Bowden, and M. A. Green, Spatially resolved analysis and minimization of resistive losses in high-efficiency Si solar cells, *Prog. Photovoltaics* **4**, 399 (1996).
- [38] D. Pysch, A. Mette, and S. W. Glunz, A review and comparison of different methods to determine the series resistance of solar cells, *Sol. Energy Mater.* **91**, 1698 (2007).
- [39] S. Schiefer, B. Zimmermann, S. W. Glunz, and U. Würfel, Applicability of the suns- V_{OC} method on organic solar cells, *IEEE J. Photovoltaics* **4**, 271 (2014).
- [40] L. J. A. Koster, V. D. Mihailetschi, H. Xie, and P. W. M. Blom, Origin of the light intensity dependence of the short-circuit current of polymer/fullerene solar cells, *Appl. Phys. Lett.* **87**, 203502 (2005).
- [41] W. Shockley and W. T. Read, Statistics of the recombinations of holes and electrons, *Phys. Rev.* **87**, 835 (1952).
- [42] R. C. I. MacKenzie, C. G. Shuttle, G. F. Dibb, N. Treat, E. von Hauff, M. J. Robb, C. J. Hawker, M. L. Chabinyk, and J. Nelson, Interpreting the density of states extracted from organic solar cells using transient photocurrent measurements, *J. Phys. Chem. C* **117**, 12407 (2013).
- [43] R. C. I. MacKenzie, A. Göritz, S. Greedy, E. von Hauff, and J. Nelson, Theory of Stark spectroscopy transients from thin film organic semiconducting devices, *Phys. Rev. B* **89**, 195307 (2014).
- [44] Y. Gao, R. C. I. MacKenzie, Y. Liu, B. Xu, P. H. M. van Loosdrecht, and W. Tian, Engineering ultra long charge carrier lifetimes in organic electronic devices at room temperature, *Adv. Mater. Interfaces* **2**, 1400555 (2015).
- [45] R. C. I. MacKenzie, General-purpose Photovoltaic Device Model—gpvdm, <https://www.gpvdm.com>.
- [46] L. A. A. Pettersson, L. S. Roman, and O. Inganäs, Modeling photocurrent action spectra of photovoltaic devices based on organic thin films, *J. Appl. Phys.* **86**, 487 (1999).